exchange process, a glass substrate was placed in a mixed melt of $AgNO_3$ and KNO_3 at 400 °C. The thickness of the glass substrate, time of the ion-exchange process, and weight concentration of $AgNO_3$ in the melt determined the concentration and distribution of Ag^+ ions in the glass. Thermal annealing of the ion-exchanged glass in a H_2 reduction atmosphere, typically at 400–450 °C, resulted in the formation of spherical silver nanoparticles [14].

Macroporous silicon with lattice constants of 500 nm or 2 μm were grown in a photoelectrochemical etching process of lithographically prestructured <100>-oriented n-type silicon wafers. In each case, the front side of the wafer was in contact with hydrofluoric acid (concentration $c_{HF} = 5$ wt.-%; $T = 10$ °C) whereas the backside was illuminated generating electron–hole pairs. An external anodic bias then consumed the electrons, and the electrons/holes diffused through the whole wafer to the silicon electrolyte interface, promoting the silicon dissolution there. The pores with very flat surfaces and high aspect ratios grew straight along the (001) direction of the silicon single crystal [15,16]. The macroporous silicon samples were then sputtered with 10 nm chromium film to avoid anodic bonding during the experiments [17,18].

Received: July 19, 2005
Final version: September 7, 2005
Published online: November 3, 2005

[1] U. Kreibig, M. Vollmer, *Optical Properties of Metal Clusters*, Springer, Berlin **1995**.
[2] V. M. Shalaev, *Optical Properties of Nanostructured Random Media*, Springer, Berlin **2002**.
[3] K. L. Kelly, E. Coronado, L. L. Zhao, G. C. Schatz, *J. Phys. Chem. B* **2003**, *107*, 668.
[4] R. C. Jin, Y. C. Cao, E. C. Hao, G. S. Metraux, G. C. Schatz, C. A. Mirkin, *Nature* **2003**, *425*, 487.
[5] M. S. Gudiksen, L. J. Lauhon, J. Wang, D. C. Smith, C. M. Lieber, *Nature* **2002**, *415*, 617.
[6] A. Moroz, *Phys. Rev. Lett.* **1999**, *83*, 5274.
[7] W. Y. Zhang, X. Y. Lei, Z. L. Wang, D. G. Zheng, W. Y. Tam, C. T. Chan, P. Sheng, *Phys. Rev. Lett.* **2000**, *84*, 2853.
[8] T. Wenzel, J. Bosbach, A. Goldmann, F. Stietz, F. Träger, *Appl. Phys. B: Lasers Opt.* **1999**, *69*, 513.
[9] F. Stietz, *Appl. Phys. A: Mat. Sci. Process.* **2001**, *72*, 381.
[10] M. Kaempfe, T. Rainer, K.-J. Berg, G. Seifert, H. Graener, *Appl. Phys. Lett.* **1999**, *74*, 1200.
[11] A. Podlipensky, A. Abdolvand, G. Seifert, H. Graener, *Appl. Phys. A: Mat. Sci. Process.* **2005**, *80*, 1647.
[12] A. Podlipensky, A. Abdolvand, G. Seifert, H. Graener, O. Deparis, P. G. Kazansky, *J. Phys. Chem. B* **2004**, *108*, 17 699.
[13] O. Deparis, P. G. Kazansky, A. Abdolvand, A. Podlipensky, G. Seifert, H. Graener, *Appl. Phys. Lett.* **2004**, *85*, 872.
[14] K.-J. Berg, A. Berger, H. Hofmeister, *Z. Phys. D: At., Mol. Clusters* **1991**, *20*, 309.
[15] V. Lehmann, *J. Electrochem. Soc.* **1993**, *140*, 2836.
[16] MPI: Ordered Porous Materials. http://www.mpi-halle.mpg.de/~porous_m/ (accessed September 2005).
[17] T. Rogers, J. Kowal, *Sens. Actuators, A* **1995**, *46*, 113.
[18] M. Despont, H. Gross, F. Arrouy, C. Stebler, U. Staufer, *Sens. Actuators, A* **1996**, *55*, 219.
[19] A. Abdolvand, A. Podlipensky, G. Seifert, H. Graener, O. Deparis, P. G. Kazansky, *Opt. Express* **2005**, *13*, 1266.
[20] G. Mie, *Ann. Phys.* **1908**, *25*, 377.

DOI: 10.1002/adma.200501305

Polymer-Reinforced, Aligned Multiwalled Carbon Nanotube Composites for Microelectromechanical Systems Applications**

By *Weileun Fang*,* *Huai-Yuan Chu*, *Wen-Kuang Hsu*, *Tung-Wen Cheng*, and *Nyan-Hwa Tai*

Carbon nanotubes have attracted much attention,[1] mainly because of their unique one-dimensional (1D) electronic properties and high tensile strength.[2] Nanotubes were first produced mostly by the arc discharge of carbon, the pyrolysis of hydrocarbons, and the laser ablation of graphite. The selective growth of aligned nanotubes was later developed, using metal-coated Si wafers as growth templates, which produce so called nanocarpets.[3] The intertube binding within carpets is relatively weak compared with the covalent character of the in-plane C–C bonds. Consequently, aligned nanotube films currently focus mainly on electronic field emission.[4] To date, the fabrication of aligned nanotube films into microelectromechanical systems (MEMS), such as suspended microbeams and -plates, remains a challenge, mainly because the intertube weakness makes them unable to carry a load in high-frequency bending maneuvers. If nanotube composites are to be made as MEMS devices, their vibration damping factor must be equivalent to that of metals. In this paper, we report on the successful development of a novel method for reinforcing intertube binding with a polymer: the nanotube composites were then fabricated into MEMS devices. Mechanical tests reveal an increase of the composite modulus by a factor of 20 compared with bare nanotubes. The damping and quality factors for nanotube MEMS devices are 12 and 0.042 at 1 atm (1 atm = 101.325 kPa), respectively, which are comparable with those of typical MEMS components.

Aligned multiwalled nanotube (MWNT) films have been grown as microgripper structures (Fig. 1b), which are well defined and commonly seen in MEMS devices. These structures were established in step II (Fig. 1a). MWNT grippers were then filled by polymer in step III, and typical examples are

[*] Prof. W. Fang, Dr. H.-Y. Chu
Power Mechanical Engineering Department
National Tsing Hua University
101, Section 2 Kuang Fu Road, Hsinchu (Taiwan)
E-mail:fang@pme.nthu.edu.tw
Prof. W.-K. Hsu, T.-W. Cheng, Prof. N.-H. Tai
Department of Materials Science and Engineering
National Tsing Hua University
101, Section 2 Kuang Fu Road, Hsinchu (Taiwan)

[**] This work was supported by the National Science Council of Taiwan (NSC-93-2218-E-007-012, NSC-93-2113-M-007-028).

ADVANCED MATERIALS

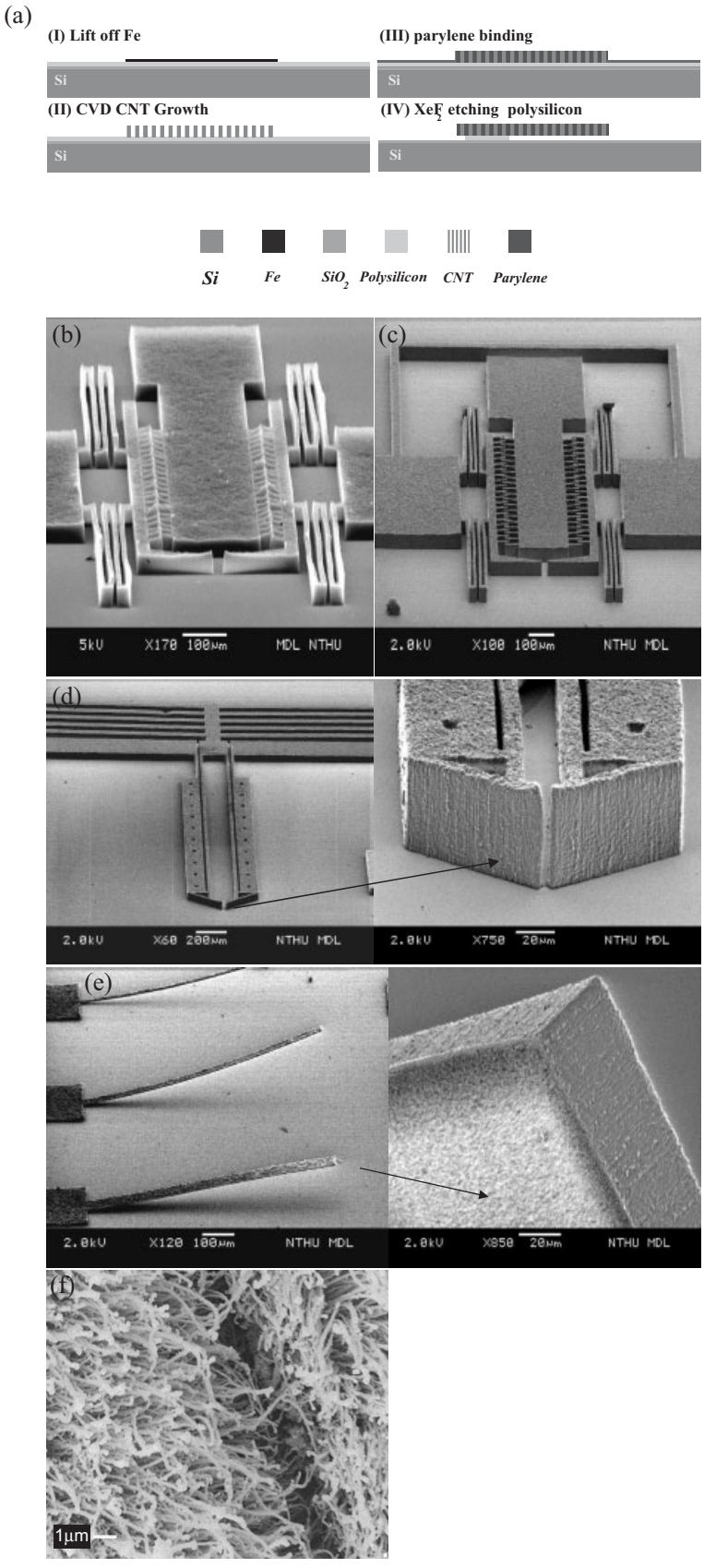

Figure 1. a) Fabrication procedure for MWNT MEMS. Scanning electron microscopy (SEM) images of b) typical microgrippers made by aligned MWNT films; c) polymer-reinforced MWNT microgrippers; d) a reinforced MWNT gripper and its gripper front; e) a suspended microbeam and its side view; f) exposure of the internal nanotubes to acidic etching of the polymer. CVD: chemical vapor deposition; CNT: carbon nanotube.

shown in Figure 1c. Polymer binding did not change the original gripper structures, including the device dimensions and shape. For example, the microtrenches, folding fences, and the gap between the grippers did not distort (Fig. 1c). The aligned wave patterns seen on the gripper surfaces possibly resulted from the underlying aligned MWNTs (arrow, Fig. 1d). In order to verify whether the polymer uniformly and thoroughly filled the intertube spaces, the underlying polysilicon layer was partially etched by vapor-phase XeF_2 to form suspended structures (step IV, Fig. 1a). Figure 1e shows suspended microcantilevers made of MWNT–polymer. The structures, which are bent upwards, were formed by the residual stress of the composite films (Fig. 1e, left).[5] We tilted the SEM sample stage by 10–20°, to observe the bases and side walls of the cantilevers (Fig. 1e, right). Scanning electron microscopy (SEM) images revealed that the bases and side walls are also solid structures, in particular, there are no polymer excrescences along the film edges. The internal MWNTs maintained their alignment well when they were coated with polymer; this was verified by partial exposure of the MWNTs to mild acidic etching (Fig. 1f).

The mechanical properties of the aligned MWNT films and polymer-reinforced MWNT MEMS were tested and compared. Material hardness was tested by commercial thin-film indentation using magnetic coils as the force induction (MTS Nano Indenter, resolution ±1 nN),[6,7] and the displacement magnitude was recorded with a capacitive displacement sensor with subnanometer resolution. Film surfaces were indented by a triangular-pyramid tip (Berkovich indenter), and the tip displacement versus load was recorded in situ. According to the conservation rule-of-thumb, the variation of material hardness with indentation depth is approximately 5–10 % of the film thickness.[7] Therefore, the measured hardness versus indentation depth was calculated within a 5 % range for hardness characterization (Fig. 2a, left). Indentation measurements gave a mean hardness of 0.005 GPa for bare aligned MWNT films, which is very low. The occurrence of collapsing edges around the indented holes points to the fact that the

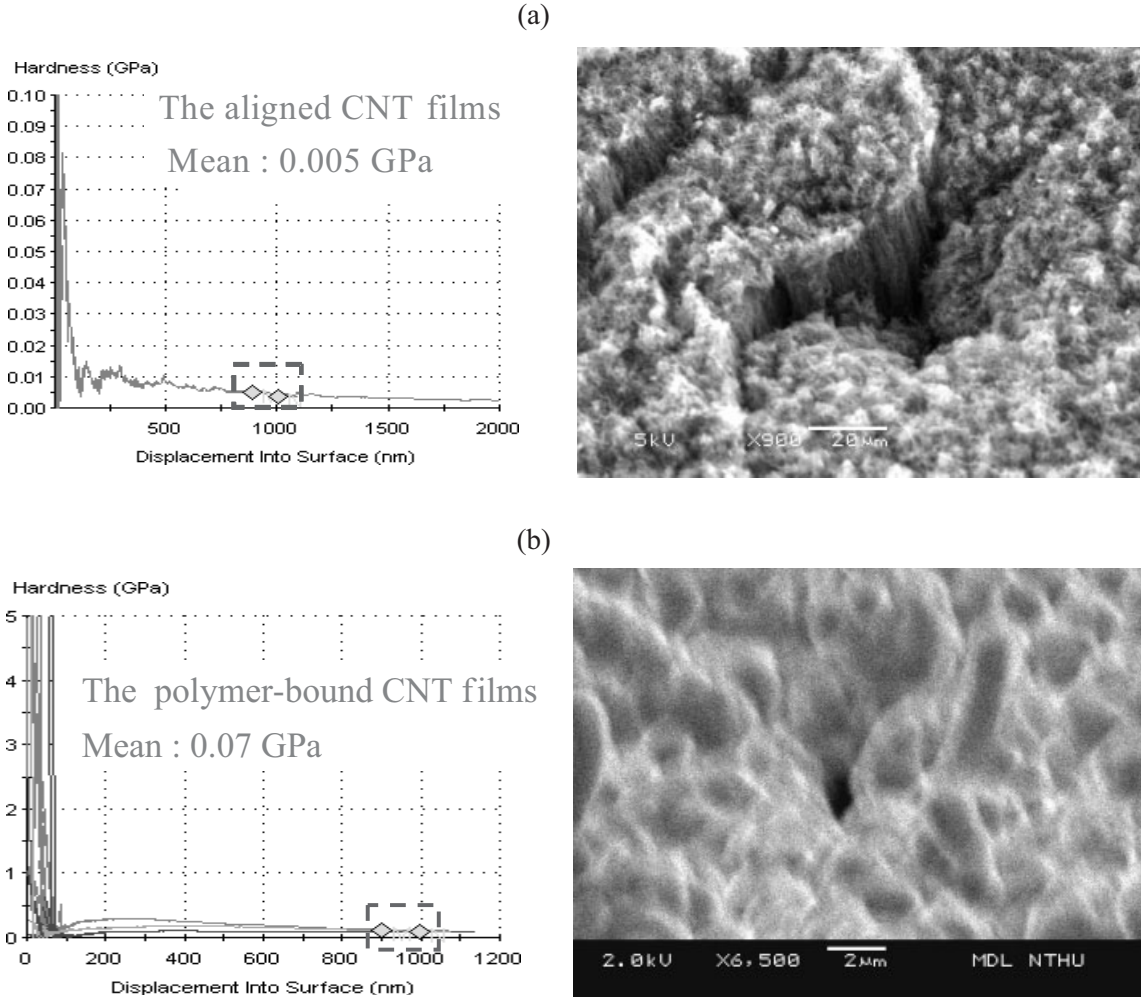

Figure 2. Indentation measurements of a) aligned MWNT films, and b) polymer-filled MWNT films. The indentation direction is parallel to the MWNT axis, and the oscillation seen at the beginning of both indentation profiles is due to surface roughness. Oscillation rapidly minimizes, and the profile levels off when the indentation depth is increased further. The images on the right are SEM images of the respective structures.

ADVANCED MATERIALS

bare, aligned MWNT films are soft surfaces (Fig. 2a, right). Similar indentation experiments gave a value of 0.07 GPa for polymer-reinforced MWNT MEMS (Fig. 2b, left), which is about fourteen times greater than bare MWNT films. The polymer-reinforced MWNT composite shows a smaller indented crack (1 μm) than the actual indenter tip (Fig. 2b, right), implying that the indented structure has recovered to some extent, and that the material is elastic. Note that the hardness of the parylene film is only 0.005 GPa.

Aligned MWNTs and polymer-filled MWNT composites were fabricated into microbridge structures consisting of a micromachined beam with both ends fixed. Figure 3a shows two typical microbridges made of aligned MWNTs, which are 20 μm thick and 20 μm wide, with beam lengths of 100 and 200 μm. The density, ρ, of the aligned MWNT film is 1.39 g cm^{-3}, a value which is similar to that of the polymer-filled MWNT composites. The elastic modulus of the bridge was determined using a resonance frequency method, as follows. The substrate with microbridges was mounted on an ultrasonic piezoelectric (PZT) transducer using wax (or sticky tape) and the PZT was driven by a function generator and power amplifier. The mounted microbridge was then vibrated with a broad-bandwidth sine sweep frequency excitation, and the corresponding dynamic response from the bridge entity was measured in situ using a commercial laser Doppler vibrometer system (LDV, Polytec Gmbh Microscope scanning vibrometer). The time versus frequency responses from the testing structures were analyzed by an oscilloscope and a frequency analyzer, respectively. According to the Euler–Bernoulli beam model,[8] the nth natural frequency of bending vibration $(f_B)_n$ and equivalent Young's modulus (E) of a microbridge are expressed by Equation 1

$$E = \frac{48\pi^2 \rho L^4 (f_B)_n^2}{(\beta_L)_n^4 h^2} \quad (1)$$

in which L and h are the length and thickness of the microbridge, respectively. The parameter $(\beta_L)_n$ is the nth eigenvalue of the equation governing the microbridge. Figures 3b,c show the frequency responses of microbridges made of an aligned nanotube film and a polymer-filled MWNT film, respectively. The first resonant frequency of the bending vibration for an aligned MWNT microbridge is 78 kHz (Fig. 3b) and the parameter $(\beta_L)_1$ for the first resonant frequency is 4.73.[8] By substituting the above numbers into Equation 1, the equivalent E value for the aligned nanotube film is 1.3 GPa. The first resonance frequency of the bending vibration for a polymer-reinforced MWNT microbridge is 351 kHz (Fig. 3c), corresponding to an E value of 26 GPa. Hence, polymer binding enhanced the E value of the microbridge by about a factor of twenty. Note that the E value of a parylene polymer film is only 3 GPa.[9]

Vibration measurements were also carried out on suspended microcantilevers. As aligned nanotubes cannot be fabricated into a suspended structure, vibration experiments were only performed on microcantilevers made of polymer-reinforced MWNT composites. The testing cantilever was 20 μm thick, 2700 μm long, and 50 μm wide (Fig. 3d). The shear modulus G for the cantilevers was evaluated according to Meirovitch,[10] and the natural frequency of the first torsional vibration mode f_T for a cantilever is expressed by Equation 2

$$G = \frac{4\rho L^2 (b^2 + h^2) f_T^2}{3 c_2 h^2} \quad (2)$$

in which b is the width of the cantilever, and the constant c_2 is a coefficient dependent on the b/h ratio. Hence, when resonance frequencies are defined, the corresponding G of the microcantilever can be quantified. Figures 3e,f show the frequency response of a suspended cantilever, ranging from 1 to 300 kHz. More than ten resonant frequencies were excited from the cantilever, and resonant peaks associated with the PZT transducer are distinct (stars). In addition to vibration tests, a finite-element model using the commercial software ANSYS has been established to predict resonance frequencies of the cantilever, for comparison purposes. This simulation was carried out by treating the MWNT composite as a continuous and homogeneous structure. Table 1 shows the first ten resonant frequencies of a cantilever measured by LDV compared with ANSYS calculations; a good agreement emerges between measured and simulated data. Equivalent E and G values, determined by bending modes and the first twisting mode, are 40 and 15.7 GPa, respectively. It is worth noting that the microbridge and microcantilever, both measured by the same procedure, yield different moduli (26 and 40 GPa); the difference is due to the deviation in film thickness. The E value of the microcantilever obtained here, however, is more accurate, because deviation of the film thickness has been minimized by repeating measurements using ten different modes.

Table 1. Comparison between experimental and calculated data over ten resonant modes for a suspended microcantilever made of MWNT composites.

Mode	1	2	3	4	5	6	7	8	9	10
ANSYS [kHz]	2.5	6.2	15.7	39.2	44.9	90.9	111.7	157.5	216.9	225.6
Experiment [kHz]	2.4	6.9	13.7	35.0	47.9	84.5	112.6	160.1	216.0	226.8

MEMS devices are frequently operated under resonant modes, so the damping factor (Q) for the MWNT MEMS devices needs to be characterized. Equation 3 was used to evaluate the Q value, based on the first bending mode $(f_B)_1$

$$Q = 1/2\zeta = (f_B)_1/\Delta f \quad (3)$$

in which Δf is the bandwidth of the mode and ζ denotes the quality factor. A good fit to Figure 3g gives $\zeta = 0.042$ and

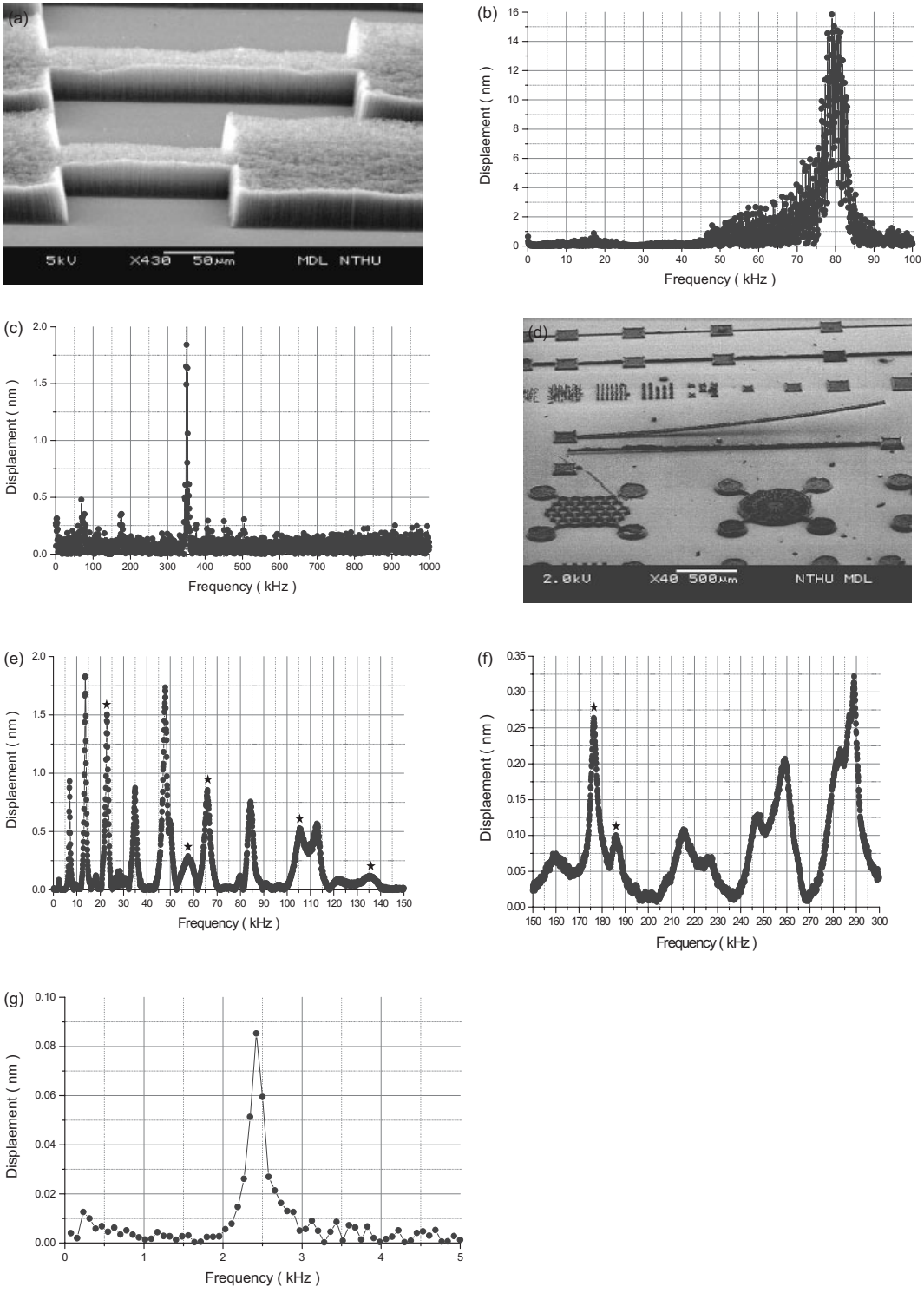

Figure 3. a) SEM image of a microbridge, and b,c) corresponding vibration frequency response for bridges made of aligned MWNTs (b) and polymer-filled MWNTs (c). d) SEM image of a suspended microcantilever made of MWNT composites. e,f) The first ten resonant frequencies of a microbridge made of reinforced MWNT composites between 0 and 140 kHz (e); and between 150 and 300 kHz (f). g) Damping profile calculated based on the first bending mode. (Note that the microbeam vibration was induced vertically).

$Q = 12$ (at 1 atm), values which are comparable with those of classical MEMS devices. Dynamic bending tests were carried out and recorded on a suspended MWNT–polymer microbeam driven by an electrostatic force with different frequencies (Figs. 4a–d). The dimensions of the suspended beam were 2700 µm × 50 µm × 20 µm, and the bending displacement for

ADVANCED MATERIALS

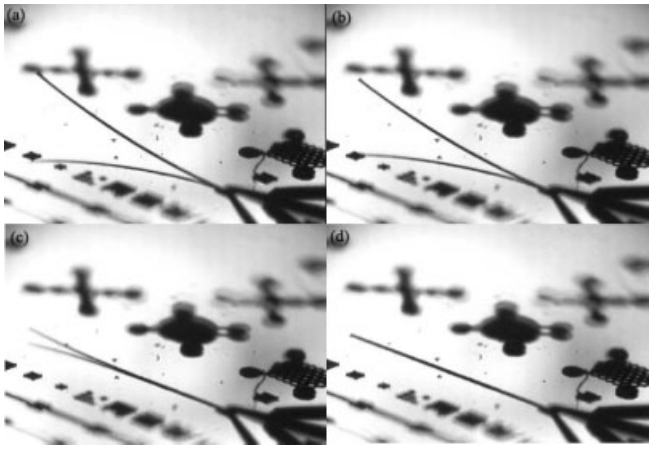

Figure 4. a–d) Snapshots of dynamic bending on a suspended microbeam.

tip-to-substrate was 560 μm. The pull-in voltage for driving the MWNT–polymer microbeam was only 50 V, which is significantly lower than that needed to drive a classical MEMS microbeam with similar structure (500 V). Note that conventional MEMS microbeams driven at 500 V normally produce a tip-to-substrate displacement below 200 μm.

MWNT–polymer composites, made by mechanical blending between nanotubes and polymers, or by polymerization in the presence of nanotubes, only lead to a random arrangement of MWNTs in the matrix. Such a system lacks packing efficiency, so the load-carrying capacity of the nanotubes is limited.[11] The MWNT–polymer composites produced here can be considered as a unidirectional, long-fiber matrix system, because the polymer mainly occupies the intertube space, and the nanotube length is equal to the composite dimension along the z direction. This novel nanotube–polymer system has several advantages. First, the matrix fractures before nanotube breakage, because the nanotube modulus is greater than that of the polymer ($E_{polymer} < E_{tube}$). Second, the MWNT pull-out mechanism is unlikely. Third, the tube-packing efficiency is maximized in the matrix. Fourth, the critical length along the filler axis for efficient load carrying approaches zero, namely the efficient length for load carrying is about the same length as the nanotube. We characterized the azimuth moduli of aligned MWNT composites as follows: the volume fraction of nanotubes in the composite is $V_{tube} = (W_1/\rho_1)/(W_1/\rho_1 + W_2/\rho_2 + W_3/\rho) = 0.5–0.6$, in which W is the weight fraction of the constituents. (Note that for MWNT–polymer materials prepared via mechanical blending $V_{tube} \approx 0.01–0.005$).[12] Using the Halpin–Tsai equations, the parallel ($E_{\|}$) and transverse ($E_{\perp}$) moduli were calculated to be 78 and 6.4 GPa respectively, where $E_{\|} = E_{tube}E_{polymer} + E_{polymer}(1–V_{tube})$, and $E_{\perp} = E_{tube}E_{polymer}/[E_{tube}(1–V_{tube}) + E_{polymer}V_{tube}]$.[13] By substituting the above values into Equation 4,

$$\nu = (E/2G)–1 \quad (4)$$

in which $E = 3E_{\|}/8 + 5E_{\perp}/8$ and $G = E_{\|}/8 + E_{\perp}/4$,[13] Poisson's ratio, ν, was calculated to be 0.19. The values of $E_{\|}$, $E_{\perp}$, and Poisson's ratio obtained here are similar to those of the carbon fiber–epoxy system,[13] which explains the significant promotion of the composite modulus in this study.

In conclusion, aligned MWNTs have been grown, and subsequently reinforced by a polymer. MWNT composites can be fabricated into MEMS devices. A nanotube-based microbeam was driven at lower pull-in voltage compared with metallic microbeams.

Experimental

The fabrication procedure established in this study is shown in Figure 1a. Step I indicates a thin film of polysilicon (lightest gray, 1 μm) deposited on top of the Si wafer (bottom layer, labeled). An Fe film (black, 30 nm) was then deposited and patterned onto polysilicon by means of a lift-off technique. Aligned MWNT films were grown by chemical vapor deposition using acetylene as the precursor at 800 °C in an Ar/H_2 flow for 10 min. Parylene was selected as the binding agent, because of its low dissipation factor, high dielectric strength, and dielectric constant, which is invariant to the frequency. The intertube space was then filled with Parylene (step II) and the filling procedure was as follows. Solid parylene dimers were first vaporized at 150 °C in a stainless steel chamber. The polymer vapor was mixed with methylene and the gas mixture was then introduced into a neighboring furnace (680 °C) to yield stable, monomeric diradical *para*-xylylene. Monomers were subsequently re-directed into a room-temperature deposition chamber where they simultaneously polymerized and adsorbed onto the MWNTs and polysilicon substrate (step III) [9]. Finally, MWNT–polymer composites were released to form suspended micromachined structures by removing the underlying polysilicon by using vapor-phase XeF_2 etching (step IV).

Received: June 25, 2005
Final version: August 31, 2005
Published online: November 3, 2005

[1] S. Iijima, *Nature* **1991**, *354*, 56.
[2] D. Qian, G. J. Wagner, W. K. Liu, M.-F. Yu, R. S. Ruoff, *Appl. Mech. Rev.* **2002**, *55*, 495.
[3] M. Terrones, N. Grobert, J. Olivares, J. P. Zhang, H. Terrones, K. Kordatos, W. K. Hsu, J. P. Hare, P. D. Townsend, K. Prassides, A. K. Cheetham, H. W. Kroto, D. R. M. Walton, *Nature* **1997**, *388*, 52.
[4] S. Fan, M. G. Chapline, N. R. Franklin, T. W. Tombler, A. M. Cassell, H. Dai, *Science* **1999**, *283*, 512.
[5] W. Fang, J. A. J. Wickert, *J. Micromech. Microeng.* **1996**, *6*, 301.
[6] H. D. Espinosa, M. Fischer, E. Herbert, W. C. Oliver, www.mts.com/downloads/100-034-533MEMS.pdf (last accessed October 2005)
[7] G. M. Pharr, W. C. Oliver, *MRS Bull.* **1992**, *7*, 28.
[8] Parylene specifications and properties, www.scscookson.com (last accessed September 2005).
[9] S. S. Rao, *Mechanical Vibrations*, 3rd ed., Addison-Wesley Publishing Company, Reading, MA **1995**.
[10] L. Meirovitch, *Analytical Methods in Vibration*, MacMillan, New York **1967**.
[11] K. T. Lau, D. Hui, *Carbon* **2002**, *40*, 1597.
[12] R. Andrews, D. Jacques, M. Minot, T. Rantell, *Macromol. Mater. Eng.* **2002**, *287*, 395.
[13] D. Hull, *An Introduction to Composite Materials*, Cambridge University Press, New York **1981**.

